Theoretical analysis of streamwise vortex circulation induced by a strut injector

Toshihiko Hiejima*

Department of Aerospace Engineering, Osaka Prefecture University, 1-1 Gakuen-cho, Nakaku, Sakai, Osaka 599-8531, Japan

(Received 5 June 2016; published 13 September 2016)

This paper presents a theoretical study of circulation of streamwise vortices that are generated by a hypermixer strut in a supersonic flow. By taking account of the spanwise velocity, the circulation based on the streamwise vorticity is derived from an inviscid flow around the strut. The theoretical circulations are in agreement with the values obtained from three-dimensional numerical simulations for small slope angles at a Mach number of 2.48. Therefore, the proposed circulation formula can contribute to designing struts, in that it depends only on the strut configuration and inflow conditions. This study also finds that the linear relations between circulation and angle is broken by separated flows on the slope wall with increasing angle and the maximum value in circulation is expressed as a product of the mainstream velocity and the height of the strut.

DOI: 10.1103/PhysRevFluids.1.054501

I. INTRODUCTION

The main issue in the field of supersonic combustion ramjet propulsion is to address effective fuel-oxidizer mixing in the engine over the short time scale of combustion [1]. To enhance mixing in supersonic flows, the use of axial vorticities, i.e., streamwise vortices, is extremely effective [2–4]. Moreover, vortex breakdown induced by an interaction between streamwise vortices and shock waves has a large effect on mixing and combustion [5–7]. The fundamental physics underpinning streamwise (axial) vortices is important because those vortices are intimately linked with instabilities and turbulent transitions. Previous work has demonstrated that flows with streamwise vortices are more unstable than those without axial vorticity. Those results are related to the fact that a crop of unstable streamwise vortices and their interactions result in a breakdown in the process of turbulent transition, as observed for low-speed flows; however, the results indicate the effectiveness of streamwise vortices at high-speed flows (see, for example, [8]). Furthermore, a streamwise vortex can entrain the surrounding air; the presence of strong axial vorticity has the benefit of greater mixing power. The entraining efficiency of streamwise vortices was also shown to be high in round jets [9].

However, with regard to the production of axial vorticities, it is difficult to produce a large swirl number, i.e., a vortex with large circulation, in supersonic flows. Thus, it is necessary to devise a way to generate streamwise vortices with loss reduction and without a complex generator for the swirl components. To decrease the loss, some strut-type injectors using a ramp device have been proposed for supersonic mixing problems [10–14]. Each strut injector has a feature designed to form streamwise vortices in the center of the mainstream (see Fig. 1), such as lobed struts [10], struts with parts parallel to the flow [11–13], and single-wedge lobed struts [14]. Moreover, it has been demonstrated that the streamwise vortices generated by those kinds of injectors play a large role in supersonic combustion at a Mach number of 2.5 [15–17].

The circulation of a streamwise vortex is a crucial indicator of the entrainment rate; therefore, the present investigation takes particular note of the formation process of the vortex. Although it is expected that the circulation generated from ramp devices depends on the height and the slope of the strut, few studies have ever investigated the relation between the circulation and slope of

*hiejima@aero.osakafu-u.ac.jp

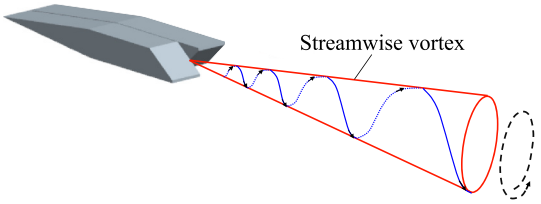

FIG. 1. Schematic of a streamwise vortex induced by a hypermixer strut.

the strut despite the importance of this relation. If circulations could be estimated with ease and accuracy, it would be more convenient to design strut injectors. In practice, a theoretical basis for the circulation estimation is required, particularly under high-enthalpy flow conditions [15] at the time of supersonic combustion.

In this paper the relation between the circulation of a streamwise vortex generated by a hypermixer strut and the slope of the strut is investigated under a high-enthalpy flow. As part of the approach, the circulation is deduced from a theoretically derived formula based on inviscid supersonic flows. The formula is validated as per the values obtained from three-dimensional (3D) numerical simulations.

II. STRUT INJECTORS TO INDUCE STREAMWISE VORTICES

Figure 2 shows the strut injector for inducing streamwise vortices in supersonic flows that is studied here; it is the same as the one commonly used in the literatures [11,12,15–18]. This strut comprises the leading edge of a symmetry wedge with a half-apex angle of 5.7°, the parallel pylon part, and the trailing edge that has asymmetrical up and down slopes, which alternate in the span direction; the width of the slope is $D = 11$ mm, the height of the strut is $H = 10$ mm, and the slope angle is θ (in degrees). Note that the length of the trailing edge $X_S = H/\tan\theta$ decreases with increasing θ. This strut is also excellent for drag because under the assumption of an inviscid flow, the drag coefficient [19] caused by shock waves is 0.0174 at the mainstream Mach number $M_\infty = 2.48$ and the loss of total pressure is approximately 1% due to the shockwave.

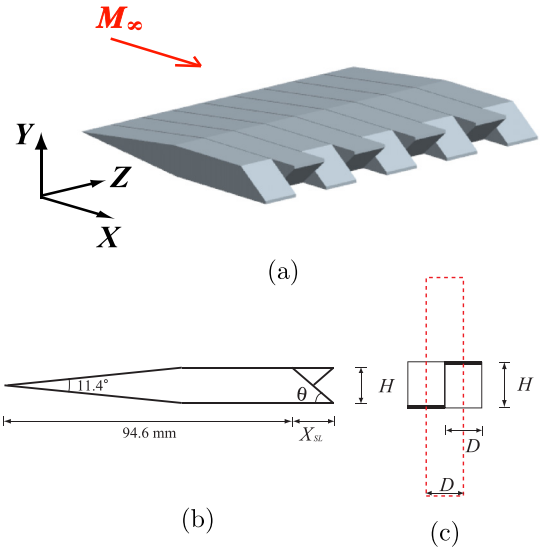

FIG. 2. (a) Schematic of a hypermixer strut, also shown from (b) the side view and (c) the rear view.

III. NUMERICAL FORMULATIONS

A. Governing equations

The governing equations are the 3D, unsteady, compressible Navier-Stokes equations in general coordinates ξ_i $(i = 1 - 3)$ and are given as follows:

$$\frac{\partial}{\partial t}\left(\frac{\boldsymbol{Q}}{J}\right) + \frac{\partial \boldsymbol{F}_i}{\partial \xi_i} = \frac{\partial \boldsymbol{F}_{vi}}{\partial \xi_i}, \tag{1}$$

$$\boldsymbol{Q} = \begin{bmatrix} \rho \\ \rho u_1 \\ \rho u_2 \\ \rho u_3 \\ e \end{bmatrix}, \quad \boldsymbol{F}_i = \begin{bmatrix} \rho U_i \\ \rho u_1 U_i + p(J^{-1}\partial\xi_i/\partial x_1) \\ \rho u_2 U_i + p(J^{-1}\partial\xi_i/\partial x_2) \\ \rho u_3 U_i + p(J^{-1}\partial\xi_i/\partial x_3) \\ (e+p)U_i \end{bmatrix}, \quad \boldsymbol{F}_{vi} = \begin{bmatrix} 0 \\ \tau_{1k}(J^{-1}\partial\xi_i/\partial x_k) \\ \tau_{2k}(J^{-1}\partial\xi_i/\partial x_k) \\ \tau_{3k}(J^{-1}\partial\xi_i/\partial x_k) \\ (u_j\tau_{kj} + q_k)(J^{-1}\partial\xi_i/\partial x_k) \end{bmatrix}, \tag{2}$$

$$J^{-1} = \frac{\partial x_1}{\partial \xi_1}\left(\frac{\partial x_2}{\partial \xi_2}\frac{\partial x_3}{\partial \xi_3} - \frac{\partial x_2}{\partial \xi_3}\frac{\partial x_3}{\partial \xi_2}\right) + \frac{\partial x_1}{\partial \xi_2}\left(\frac{\partial x_2}{\partial \xi_3}\frac{\partial x_3}{\partial \xi_1} - \frac{\partial x_2}{\partial \xi_1}\frac{\partial x_3}{\partial \xi_3}\right) + \frac{\partial x_1}{\partial \xi_3}\left(\frac{\partial x_2}{\partial \xi_1}\frac{\partial x_3}{\partial \xi_2} - \frac{\partial x_2}{\partial \xi_2}\frac{\partial x_3}{\partial \xi_1}\right),$$

$$U_i = \left(J^{-1}\frac{\partial \xi_i}{\partial x_k}\right)u_k, \tag{3}$$

where $\boldsymbol{Q}$ is a vector of conservative variables and $\boldsymbol{F}_i$ and $\boldsymbol{F}_{vi}$ contain the convective and viscous fluxes, respectively. The Jacobian J transforms the coordinate system from physical space to computational space, $J^{-1}\partial\xi_i/\partial x_k$ are the derivatives for the coordinate conversion, i.e., the metrics, and U_i are the velocity components at the cell interface in general coordinates. Further, ρ is the density, u_i are the velocity components in Cartesian coordinates, e is the total energy, p is the static pressure, τ_{ij} is the viscous stress tensor, and q_i is the conductive heat flux. In these expressions,

$$\begin{aligned} p &= \rho R T e = \frac{p}{\gamma - 1} + \frac{1}{2}\rho u_k u_k, \\ \tau_{ij} &= \mu(T)\left(\frac{\partial u_i}{\partial x_j} + \frac{\partial u_j}{\partial x_i} - \frac{2}{3}\delta_{ij}\frac{\partial u_k}{\partial x_k}\right), \\ q_i &= -\kappa(T)\frac{\partial T}{\partial x_i}, \end{aligned} \tag{4}$$

where T is the static temperature and R is the gas constant. The viscosity μ and the thermal conductivity κ are calculated according to Sutherland's law

$$\mu(T) = \mu_\infty\left(\frac{T}{T_\infty}\right)^{3/2}\frac{T_\infty + \vartheta}{T + \vartheta}, \tag{5}$$

$$\kappa(T) = \frac{\mu(T)C_p}{\mathrm{Pr}}, \quad C_p = \frac{\gamma}{\gamma - 1}R, \tag{6}$$

where $\mu_\infty = 3.64 \times 10^{-5}$ Pa s, $\vartheta = 110.4$ K, $R = 287$ J/kg K, and the Prandtl number is $\mathrm{Pr} = 0.72$ for air.

B. Numerical methods and computing conditions

The purpose of this study is to capture a large-scale structure (streamwise vortex) in a complex flow field including shock waves rather than estimating quantitative small scales in their fully developed states. In that regard, the large-scale vortical structures are resolved on a sufficient number of grids based on the relation between the circulations obtained from these simulations and the total number of grid points listed in Table I.

TABLE I. Normalized circulation and grid points.

Total grid points	Normalized circulation
739500	0.865
2068500	0.754
15470000	0.703

The numerical method used here is a kind of shock-capturing scheme. The convective flux terms are evaluated using a third-order total variation diminishing scheme [20]. The viscous flux terms are calculated to second-order accuracy using a central difference method. The temporal integration adopts a lower and upper alternating direction implicit method. Turbulence models are not used because the models may have harmful effects on static pressure at a vortex's center [21] and on the circulation, which are both important in this study. Laminar simulations (as strict conditions) have an advantage in the design of strut injectors for inducing streamwise vortices, because laminar states on the strut wall provide an easy opportunity to generate separated flows compared with turbulent states, which are robust over separation. Thus, if separation does not occur under laminar conditions, it will not occur under turbulent conditions. It is intended that a streamwise vortex can be formed using strut injectors without problems.

The computational domain has a shape corresponding to that of the supersonic combustion test [15], which was performed at the Japan Aerospace Exploration Agency, as shown in Fig. 3. The strut is located in the center of the wind tunnel, which is 50 mm in height (with an expansion angle of 1.72° in the downstream direction). Figure 4 shows a lateral view of the mesh: the vertical section [Fig. 4(a)] and in the vicinity of the intersection of the slopes [Fig. 4(b)]. The mesh around the strut was formed by solving the elliptic partial differential equation with regard to orthogonality, $343 \times 282 \times 160$, in parts, $197 \times 210 \times 50$. Note that the X-coordinate origin is the trailing edge of the strut; the coordinate axes are described in Fig. 2(a). For the spanwise direction, the domain consists of the length from half of the down ramp to half of the up ramp, i.e., a streamwise vortex is included, based on the symmetry shown in Fig. 2(c).

The inflow is fixed to the values listed in Table II (high-enthalpy flow conditions [15] for the combustion test) and the outflow condition is extrapolated to zeroth order. The slip condition is assumed on the up and down walls of the wind tunnel. As described above, a symmetric boundary condition is applied to the X-Y boundary surfaces in the span direction. The boundary of the strut wall is considered to have unsteady, adiabatic, and nonslip conditions. To verify the theoretical circulation of the streamwise vortices derived in Sec. V, numerical simulations are conducted for eight values of the slope angle θ at a Mach number of 2.48.

C. Comparison between the present simulations and cold flow measurements

To compare with measurements, a flow field around a strut with a slope angle of 22° is calculated at $M_\infty = 2.45$. Another wind tunnel is used here; its measurement area is 80×80 mm^2 and the

TABLE II. Inflow conditions (vitiated airstream).

Inflow condition	Value
Mach number	$M_\infty = 2.48$
velocity	$U_\infty = 1836$ m/s
density	$\rho_\infty = 0.137$ kg/m^3
static pressure	$p_\infty = 0.058$ MPa
static temperature	$T_\infty = 1329$ K
ratio of specific heat	$\gamma = 1.28$
unit Reynolds number	$\mathrm{Re}_{\mathrm{unit}} = 6.9 \times 10^6$ m^{-1}

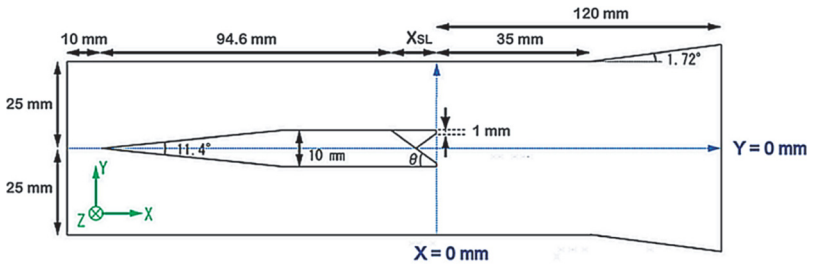

FIG. 3. Configuration of the computational domain.

experimental conditions are listed in Table III. At $X = 22$ and 35 mm, the measurements are subject to the effect of reflected separation shock waves due to interactions between shock waves occurring from the leading edge of the strut and boundary layers on the wind tunnel. Since it is hard to resolve the boundary-layer separation at the wall owing to the interaction with the shockwave, i.e., shock-wave–boundary-layer interaction [22], in terms of the calculated load, the numerical boundary condition at the wind tunnel walls is used as a slip wall; thus, the state of shock waves reflected on the walls differs in the experiments and must have slightly shifted. Figure 5 shows a comparison of the simulation and measurement results for the streamwise mass flux ρU (kg/m^2 s) at $X = 10$, 22, and 35 mm. The qualitative profiles nearly match with the measurements and these comparisons are also quantitatively matched at $X = 10$ mm, where the reflected shock waves do not impinge on the streamwise vortex.

IV. NUMERICAL RESULTS AND DISCUSSION

A. Streamwise vortices obtained from 3D numerical simulations

First, streamwise vortices are discussed based on the numerical results. Figure 6 shows the results of the numerical simulation at $\theta = 36°$: Figure 6(a) shows the contours of the schlieren images at $Z = 0$ mm of the cross plane of the up and down slopes through the center of a streamwise vortex; Fig. 6(b) shows the contours of the images at $Z = D/2 = 5.5$ mm of the middle surface of the up slope; Fig. 6(c) shows the isosurface of the second invariant of the velocity gradient tensor [23], which is often used to visualize vortical structures; and Fig. 6(d) shows the axial vorticity contours in several surfaces perpendicular to the mainstream between $X = -10$ and 40 mm. In Figs. 6(c) and 6(d) positive and negative axial vorticities are rendered in red and blue, respectively.

This paragraph outlines the streamwise vortex formation induced by the strut set in the supersonic flows. Figure 6(a) shows that a streamwise vortical structure is sharply etched behind the strut. Moreover, Fig. 6(b) shows that separation occurs at the lower end of the strut, where the expansion waves are present. In Figs. 6(a) and 6(b) the two shock waves emitted from the leading edge of

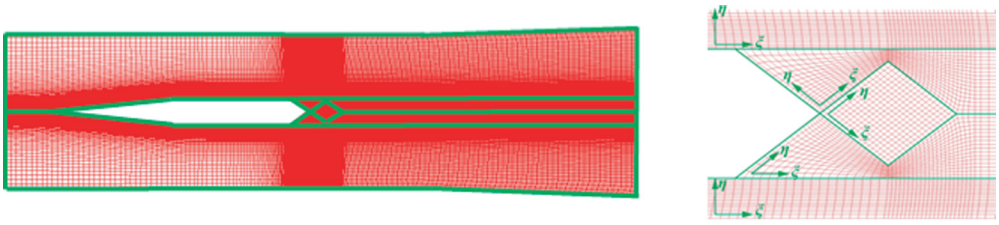

(a) (b)

FIG. 4. Lateral view of configuration of the mesh: (a) vertical section and (b) vicinity of the intersection of slopes.

TABLE III. Inflow conditions in a cold flow experiment.

Inflow condition	Value
Mach number	$M_\infty = 2.45$
velocity	$U_\infty = 562$ m/s
density	$\rho_\infty = 0.170$ kg/m^3
static pressure	$p_\infty = 6.409$ kPa
static temperature	$T_\infty = 130.9$ K
ratio of specific heat	$\gamma = 1.4$
unit Reynolds number	$\mathrm{Re}_{\mathrm{unit}} = 1.058 \times 10^7$ m^{-1}

the strut are reflected at the wind tunnel and the parallel part of the strut. Figure 6(c) shows that a large-scale vortical structure, i.e., a streamwise vortex, is formed by the strut and a double-shear layer occurs at each trailing edge, i.e., at the top and bottom surfaces of the slope. Figure 6(d), which shows the vertical planes in the stream, also confirms that a streamwise vortex with positive vorticity results from the vorticity streaming through the top surface of the slope. This process is consistent with what is depicted in Fig. 6(c). Additionally, it is found that the positive and negative vorticities in the shear layers are caught up in a streamwise vortex bent by its own rolling effect. Although the result differs from the literature [11] for a small slope angle $\theta = 10^\circ$, the same vortical structure was experimentally observed in ramp-based vortex generators [13]. Notice that negative vorticities caused by the separation appear around the positive vorticity. The helicity is approximated as $h \approx u_1\omega_1$ when u_1 is larger than other velocity components. If the streamwise vorticity is locally negative $\omega_1 < 0$, then the helicity $h < 0$, provided u_1 is positive, so that a sufficient condition for linear instability is satisfied [24]. Thus, the presence of negative vorticity may be related to the helicity instability over $X = 10$ mm where the streamwise vortex has been formed. This has an important consequence for mixing.

The separation occurs because of a pressure rise in the direction of the main flow [25]. However, it is difficult to predict how large an adverse pressure gradient has to be to generate a separated flow on the slope [26], particularly because it depends on the 3D boundary layer. Figure 7 shows the contours of shear stress on the strut wall at $\theta = 15^\circ$ and 45°. This shear stress $\tau_{\eta\xi}$ is defined as the component along a flow acting on the vertical surface of the wall; $\eta = \xi_2$ and $\xi = \xi_1$ in general coordinates. The separation region is rendered in blue (negative shear stress). It is found that flows on the parallel parts of the strut separate because of the reflected shockwave. For obvious reasons, when $\theta = 15^\circ$, no separation occurs on the slope, whereas at $\theta = 45^\circ$, the flow is separated there. To check the separation, the maximum and minimum values of the X component of the velocity in the Y-Z cross section are shown in Fig. 8. When $\theta = 22^\circ$, the velocity u_1/U_∞ is positive over the range

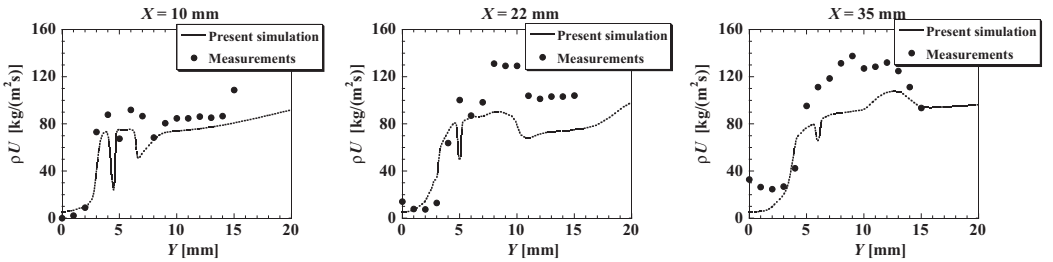

(a) (b) (c)

FIG. 5. Comparison of simulation results with cold flow experiments [the streamwise mass flux ρU (kg/m^2 s)] for a slope angle of 22° at $M_\infty = 2.45$: (a) $X = 10$ mm, (b) $X = 22$ mm, and (c) $X = 35$ mm.

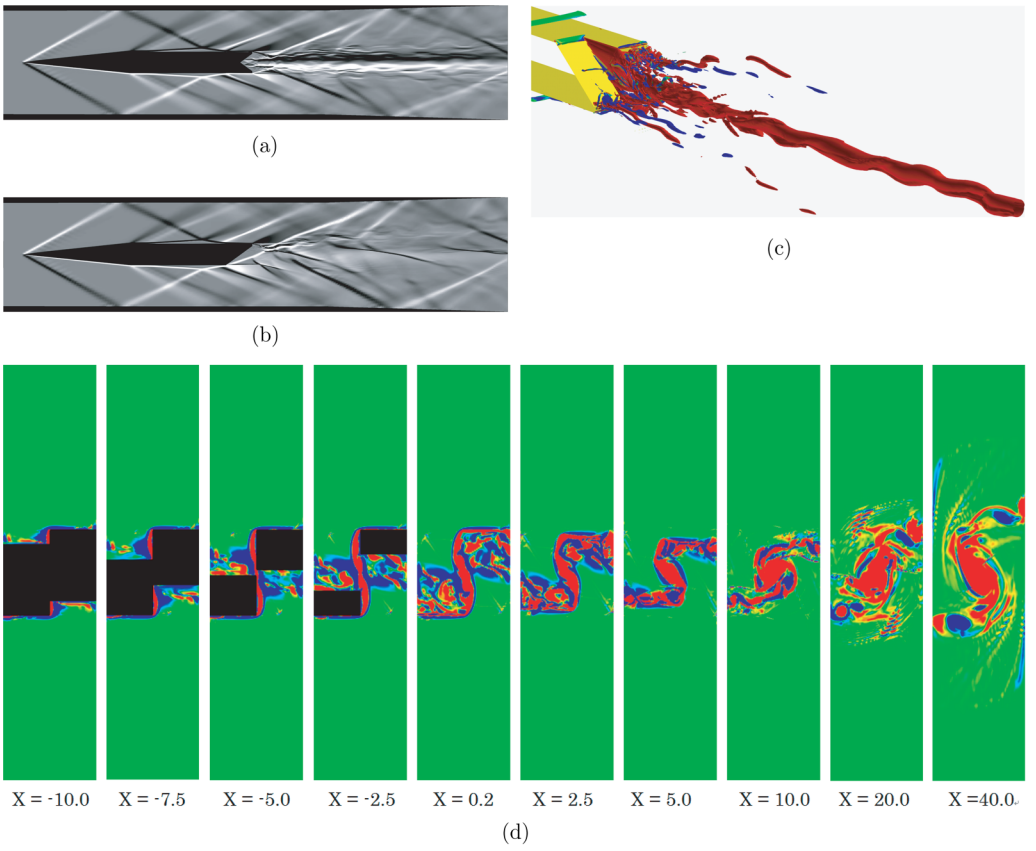

FIG. 6. Numerical simulation results for the generation process of a supersonic streamwise vortex behind a hypermixer strut with a slope angle of $\theta = 36^\circ$ at $M_\infty = 2.48$. Side views of schlieren images are shown for (a) $Z = 0$ mm and (b) $Z = 5.5$ mm. Also shown are (c) the isosurface of the second invariant of the velocity gradient tensor and (d) contours of the axial vorticity in a plane perpendicular to flow; positive and negative axial vorticities are rendered in red and blue, respectively.

$-1 < X/X_S < 0$ and when $\theta = 36^\circ$ and 45°, both the minimum velocities are negative over the range $-1 < X/X_S < 0$. These represent reverse flows at the slope, i.e., the separations occur there.

B. Circulation properties of the streamwise vortex

Circulations of streamwise vortices generated by the strut are conserved except in the case of impinging shock waves at a high Reynolds number (Kelvin's circulation theorem). As mentioned in Sec. III B, this study did not use turbulent models that are susceptible to swirl and separation

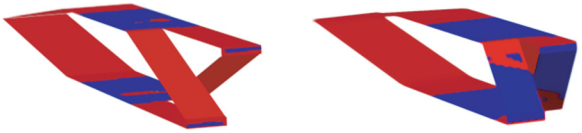

FIG. 7. Contours of shear stress on the strut wall: (a) $\theta = 15^\circ$ and (b) $\theta = 45^\circ$. Separation and nonseparation are rendered in blue (negative shear stress) and red (positive shear stress), respectively.

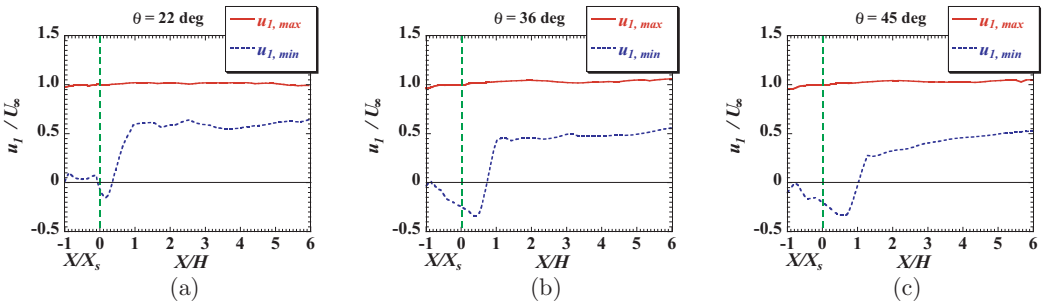

FIG. 8. Maximum and minimum values of the streamwise velocity u_1 as a function of X/X_S and X/H: (a) $\theta = 22^\circ$, (b) $\theta = 36^\circ$, and (c) $\theta = 45^\circ$.

(e.g., one of the issues is that circulations are not preserved in swirling flows). The circulation of the streamwise vorticity ω_1 is calculated by the following equation:

$$\Gamma = \int_A \omega_1 dA, \tag{7}$$

where A is the cross-sectional area in a plane perpendicular to the inflow. Figure 9 shows the streamwise variations in circulations [Figs. 9(a) and 9(b)] and the relation between circulation and slope angle [Figs. 9(c) and 9(d)]. The horizontal axis X in Figs. 9(a) and 9(b) is normalized by X_S ($X < 0$) and H ($X \geqslant 0$), respectively. In Fig. 9(a) each circulation obtains an almost uniform value at $X > 10$ mm, where the streamwise vortex formation has closed. Each enstrophy has no extremum downstream [27] and the minimum value of the streamwise velocity in Fig. 8 also remain unchanged there. Therefore, the formation of the streamwise vortex is not influenced by impinging the reflected shock waves with the deflection. In the present study, the fact that the shock waves have no impact on the vortex is consistent with the result presented in Ref. [7] based on the Mach number and shock angle. The generated circulation has the largest value at $\theta = 22^\circ$. The angle of the maximum circulation is close to that of the lobed strut at $M_\infty = 2.0$ [10].

To understand the generated circulation in detail, the circulations are divided according to the sign of their vorticity (positive or negative) $\Gamma = \Gamma^+ + \Gamma^-$, as shown in Fig. 9(b). The positive circulation increases with angle until $\theta = 22^\circ$. When θ is large, a negative circulation is formed at the slope, $-1 < X/X_S < 0$. The symbols in Figs. 9(c) and 9(d) represent circulations that are spatially averaged from $X = 10$ to 50 mm using time-averaged data. Their vertical axes Γ are normalized by $U_\infty H$. In Fig. 9(c) the positive circulations Γ^+ are nearly identical at $\theta = 22^\circ$–36°, while Γ^+ decreases when the angle becomes larger than $\theta = 36^\circ$, i.e., $\theta = 45^\circ$ and 55°, owing to separation at the slope wall. Note that the circulation for large θ may reduce the accuracy of the value with regard to the resolution of strong separation. However, as described later, the qualitative assertion that the positive circulation decreases when θ is sufficiently large seems to be reasonable. Based on the results shown in Fig. 9(c), Fig. 9(d) shows that the relation between circulation and slope angle is classified into three domains. For case A, Γ is proportional to θ. Although separation at the slope wall occurs in both cases B and C, those cases are found to differ in the formation pattern of the streamwise vortices and the tendency of Γ^+. Therefore, it is important to interpret the streamwise vortex in terms of positive and negative circulations.

The features of the formation of streamwise vortices are summarized as follows. In domain A, for a small slope angle, vortices are generated via flow to the low-pressure region on the slope from the high-pressure region on the top surface, as shown in Figs. 10(a). Thus, the formed circulation value is decided. In other words, it means that the spanwise velocity in circulation cannot be disregarded. In domain B, although the negative circulation caused by separation increases with increasing slope angle, the positive circulation is nearly unchanged and the formation pattern is similar to that in domain A. However, if the angle is in domain C, the formation process differs from that of the small

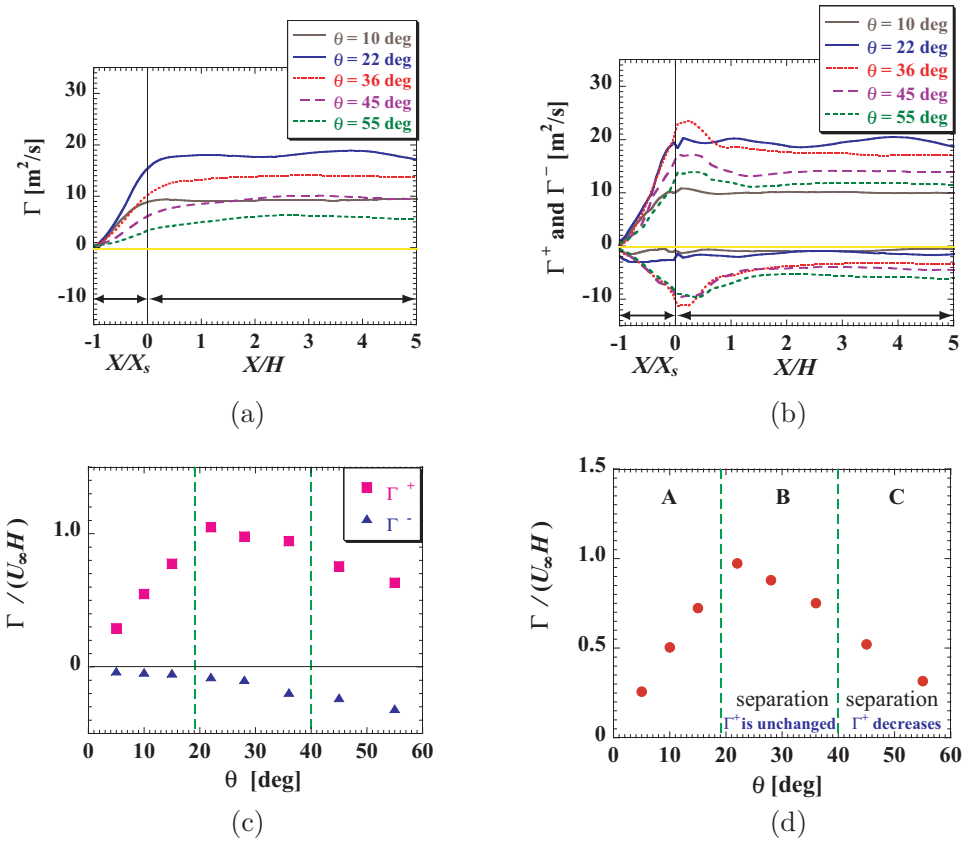

FIG. 9. Streamwise variations in circulations (a) Γ and (b) Γ^+ and Γ^- and the relation between circulation and slope angle (c) Γ^+ and Γ^- and (d) Γ.

angle. The large separation weakens the circulations that are caused by flow from the parallel part, as shown in Fig. 10(b). The reason is that the deflected flow at the corner of the beginning of the slope, which is caused by strong separation, causes the net angle to be small. Therefore, the positive circulation decreases. Subsequently, the axial vorticity component (which occurs when separation shear layers float on the separation region) becomes dominant compared to the vorticity caused by the spanwise flow (which is dominant when the slope angle is small). Thus, in this domain, the total circulation weakens as the angle increases. It is expected that the formed axial vorticities become

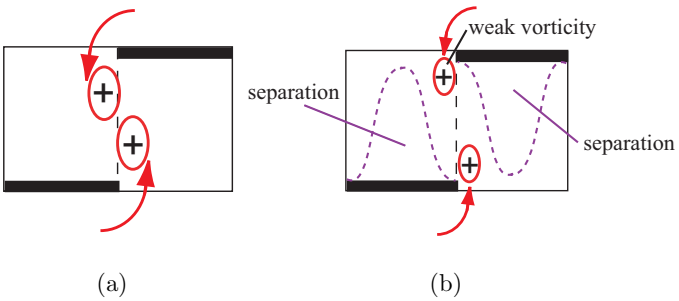

FIG. 10. Schematic of the formation process of streamwise vortices induced by a strut (a) when the angle θ is small (without separation) and (b) when the angle θ is large (with separation).

close to those formed by a based-type strut [15], wherein the rear wall is normal to the stream and the mixing property is low.

C. Mixing transition of streamwise vortices

In the design of a mixer strut, the circulation might provide a useful index of turbulent mixing. At a Mach number of 2.5, the flow fluctuation spectra that indicate transition to a developing turbulent flow were measured in streamwise vortices induced by a strut with an alternating asymmetric wedge [12]. Further, the states were satisfied with $\mathrm{Re}_\Gamma = \Gamma/\nu_\infty = 9.2 \times 10^4$, where ν_∞ is the kinematic viscosity. Dimotakis [28] proposed a mixing transition based on the fact that a leading Reynolds number has to be above a certain value to produce 3D vortical structures essential for the maintenance of turbulent mixing. The transition condition to develop a turbulent flow is that the Reynolds number must be above $(1–2) \times 10^4$, which is derived from various incompressible turbulent flows. (For the Richtmyer-Meshkov instability flow, the definition of Reynolds number is based on the large-scale vortical structure circulation and the Re_Γ is used.) According to the threshold, it is interesting to note that the streamwise vortices formed from this strut hold the potential of producing turbulent fields. To identify with this, it is necessary to simulate a counterrotating pair streamwise vortices [29,30] generated from the struts. This valuable turbulence problem remains to be clarified in compressible flows.

V. FORMULA FOR EVALUATING THE CIRCULATION OF STREAMWISE VORTICES

A. Estimation of circulations

Flows are laminar on the apex angle of the leading edge and the parallel part in a hypermixing strut at a Mach number of 2.5 [12] and separation-free along the wall surface if the slope angle θ is small. Therefore, it is expected that the circulations of streamwise vortices induced by the strut injector depend on θ, provided H is fixed. Assuming that a flow field is inviscid, the apex angle of the strut is small and the strut is parallel to the flow, the flow on the parallel part is the same as the inflow conditions listed in Table II. In this way, the equations in this section estimate the circulation of the streamwise vortex formed by the up and down ramps at the rear of the strut.

Figures 11(a) and 11(b) show a conceptual diagram of the flow field around the rear of a strut. The expressions in regions I, II, and III are denoted by subscripted variables ∞, SL, and III, respectively. Note that region IV is the same as region I, based on the inviscid assumption. The integral path and velocity components V and W required to estimate the circulation are shown in Fig. 11(c). First, the Prandtl-Meyer function, which is used across expansion waves between regions I and II, is given by

$$\nu(M_i) = \sqrt{\frac{\gamma+1}{\gamma-1}}\tan^{-1}\sqrt{\frac{\gamma-1}{\gamma+1}\left(M_i^2-1\right)} - \tan^{-1}\sqrt{M_i^2-1}, \tag{8}$$

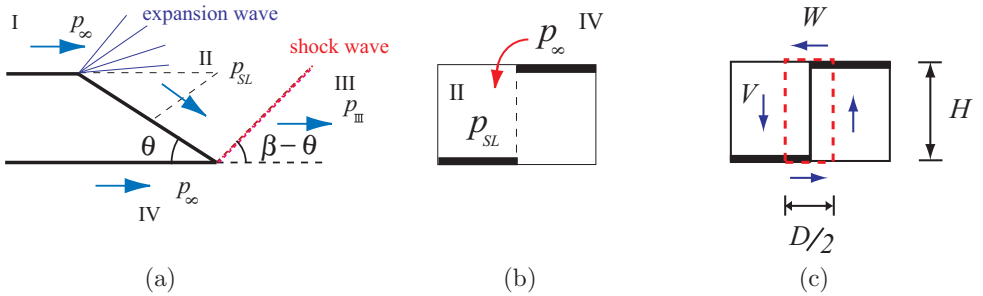

FIG. 11. Conceptual diagram of an inviscid supersonic flow around a hypermixer strut: (a) side view, (b) rear view, and (c) an integral path of the circulation.

where M_i is the local Mach number and γ is the ratio of the specific heats. Further, M_{SL} is iteratively calculated using both Eq. (8) and the expression $\nu(M_{SL}) = \nu(M_\infty) + \theta$. The speed of sound c_{SL} is

$$c_{SL} = \sqrt{\gamma \frac{p_{SL}}{\rho_{SL}}}. \tag{9}$$

As the change from region I to II is isentropic, the pressure p_{SL} and the density ρ_{SL} in region II are

$$p_{SL} = p_\infty \left(\frac{1 + \frac{\gamma-1}{2} M_\infty^2}{1 + \frac{\gamma-1}{2} M_{SL}^2} \right)^{\gamma/(\gamma-1)}, \tag{10}$$

$$\rho_{SL} = \rho_\infty \left(\frac{1 + \frac{\gamma-1}{2} M_\infty^2}{1 + \frac{\gamma-1}{2} M_{SL}^2} \right)^{1/(\gamma-1)}, \tag{11}$$

respectively. Since the velocity in the vertical direction V depends on the velocity vector and angle in region II, an expression for V can be determined from Eqs. (8)–(11) and is given as follows:

$$V = U_{SL} \sin\theta = M_{SL} c_{SL} \sin\theta, \tag{12}$$

where U_{SL} is the velocity in the stream direction in region II. Supposing that the velocity in the span direction W is caused by the difference in pressure between regions II and IV, as shown in Fig. 11(b), Eqs. (13) and (14) are obtained using the same solution as was used in the shock tube problem [31]:

$$W = \frac{2c_\infty}{\gamma - 1} \left[1 - \left(\frac{p'}{p_\infty} \right)^{(\gamma-1)/2\gamma} \right], \tag{13}$$

$$\frac{p'}{p_\infty} = \left\{ 1 - \frac{\gamma - 1}{2\gamma} \frac{\frac{c_{SL}}{c_\infty} \left[\left(\frac{p'}{p_{SL}} \right) - 1 \right]}{\sqrt{1 + \frac{\gamma+1}{2\gamma} \left[\left(\frac{p'}{p_{SL}} \right) - 1 \right]}} \right\}^{2\gamma/(\gamma-1)}, \tag{14}$$

where p' denotes a pressure that goes down through expansion waves from region IV and is iteratively calculated in Eq. (14) and then W is obtained from Eq. (13). Thus, if the path of the line integral in Fig. 11(c) is set, the circulation Γ_{th} is obtained:

$$\Gamma_{\text{th}} = 2\left(VH + W\frac{D}{2} \right). \tag{15}$$

Equation (15) indicates that the circulation depends on the inflow conditions and strut configuration (i.e., inflow Mach number and a strut's height, width, and slope angle). Furthermore, when $\theta \ll 1$ and using an expansion in terms of θ, the following relations are satisfied:

$$\frac{p_{SL}}{p_\infty} \simeq 1 - \frac{\gamma M_\infty^2}{\sqrt{M_\infty^2 - 1}}\theta, \tag{16}$$

$$\frac{p'}{p_{SL}} \simeq 1 + \frac{c_\infty}{c_\infty + c_{SL}} \frac{\gamma M_\infty^2}{\sqrt{M_\infty^2 - 1}}\theta. \tag{17}$$

Therefore, approximating Eqs. (12)–(14) on the condition that the slope angle is sufficiently small, V and W can be rewritten as follows:

$$V \simeq M_{SL} c_{SL} \theta, \tag{18}$$

$$W \simeq \frac{c_\infty c_{SL}}{c_\infty + c_{SL}} \frac{M_\infty^2}{\sqrt{M_\infty^2 - 1}}\theta. \tag{19}$$

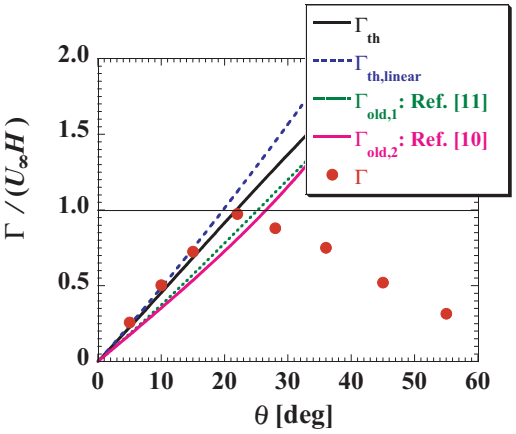

FIG. 12. Relation between the circulation and the slope angle: Circulation values were obtained from numerical simulations (red closed circles); also shown are the theoretical lines of Γ_{th} (black solid line) and $\Gamma_{\text{th,linear}}$ (blue dashed line), based on the present formulas, and the conventional estimations $\Gamma_{\text{old},1}$ (green dotted line) and $\Gamma_{\text{old},2}$ (pink solid line).

Equations (18) and (19) almost linearly depend on θ. By substituting these into Eq. (15), the circulation $\Gamma_{\text{th,linear}}$ is given as follows:

$$\Gamma_{\text{th,linear}} = K\theta, \tag{20}$$

$$K = 2M_{SL}c_{SL}H + \frac{c_\infty c_{SL}}{c_\infty + c_{SL}} \frac{M_\infty^2}{\sqrt{M_\infty^2 - 1}} D, \tag{21}$$

where K is a constant.

B. Relation between circulation and slope angle

Until now, by neglecting the spanwise flow, the circulation of streamwise vorticity based on a velocity slip in the vertical direction has been simply estimated using the following equation [11,18]:

$$\Gamma_{\text{old},1} = 2VH = 2U_{SL}H\sin\theta. \tag{22}$$

This is nearly the same as $\Gamma_{\text{old},2} = 2U_\infty H\tan\theta$ used for a lobed-mixer strut [10], where U_∞ is the velocity of the mainstream and takes no account of the spanwise velocity W. The estimate offered by Eq. (22) does not agree with circulations generated in experiments [13–15] and simulations [18] with strut injectors. Therefore, the conventional equation is unsatisfactory in terms of accuracy and is also not validated for large angles, i.e., strong circulations.

Figure 12 illustrates a comparison between the circulation values obtained from numerical simulations and those obtained from the theoretical formulas in Sec. V. As mentioned above, the conventional equation (22) underestimates the circulations. For the case where the slope angle is small, the theoretical line given by Eq. (15) is consistent with the numerical values. Additionally, the approximate equation (20) is also similar to Eq. (15). Therefore, the circulation is readily evaluated in domain A without separation. Also, the numerical results suggest that $\Gamma_{\max} \approx U_\infty H$ and the height of the strut H might be comparable to the integral length scale of the elliptic streamwise vortices formed without separation. Thus, it is extremely important to express the circulation as $\Gamma/U_\infty H$. In previous studies, $\Gamma/U_\infty H$ was 0.274 [14], 0.32 [13], and 0.35 [11] for a slope angle of 10° and 0.54 for the high-angle lobed mixer [10] at 22°. Since these values fall into the linear region in Fig. 12,

the devices from the literature can increase the circulation value by increasing the angle. It follows that the formula derived in this study is useful for designing of strut injectors.

VI. CONCLUSION

This study proposed theoretically derived circulations for supersonic streamwise vortices induced by strut injectors. In terms of strut design, it is important to consider the advantage of supersonic laminar flows in the sense that if the flow has turbulence on the wall of strut, then the desired circulation value is robustly generated by the strut, because the state is resistant to separated flows. For the case where the slope angle of the strut is small, the circulation of a streamwise vortex that is evaluated from an inviscid flow around the strut is proportional to the strut's slope angle. However, the linear relation between the circulation and the angle is broken by separation on the slope wall as the angle increases. Subsequently, the author realized that the circulation takes a downward turn owing to the negative vorticities that originated from that separation. In the linear region, the theoretical results are validated using 3D numerical simulations and the maximum value for the circulation is suggested to be expressed as a product of the mainstream velocity and the height of the strut in the present strut. Accordingly, the proposed formula can contribute to strut design, wherein the circulation solely depends on the strut configuration and inflow conditions.

From a mixing perspective, to generate the breakdown of streamwise vortices and cause speedy turbulent transitions, the presence of negative vorticity becomes a key element [32–35]. In domain A, negative circulation was rarely achieved. In domain C, although the negative circulation was large, the positive circulation was small; hence, the net circulation was weak, i.e., the entrainment rate was low. If the separation was strong during the vortex formation stage, streamwise vortices with large circulation could not be generated, e.g., $\theta = 45^\circ$ and 55°. However, at $\theta = 36^\circ$ in domain B, both the positive and negative circulations were relatively large and the formed vortex had a state of enwinding negative vorticities around a positive vorticity, as shown in Fig. 6(d). This result provides a favorable small-scale structure for mixing enhancement [33,34]. Therefore, it is important to consider the mixing powers in terms of the positive and negative vorticities.

ACKNOWLEDGMENTS

The author is grateful to Emeritus Professor M. Nishioka, Professor T. Arai, S. Sakaue, T. Sunami, and K. Komada for helpful information on supersonic measurements and thanks T. Ono for his assistance in addressing the numerical simulation and its postprocessing.

[1] E. T. Curran, W. H. Heiser, and D. T. Pratt, Fluid phenomena in scramjet combustion systems, Annu. Rev. Fluid Mech. **28**, 323 (1996).

[2] E. J. Gutmark, K. C. Schadow, and K. H. Yu, Mixing enhancement in supersonic free shear flows, Annu. Rev. Fluid Mech. **27**, 375 (1995).

[3] J. W. Naughton, L. N. Cattafesta, and G. S. Settles, An experimental study of compressible turbulent mixing enhancement in swirling jets, J. Fluid Mech. **330**, 271 (1997).

[4] K. B. M. Q. Zaman, M. F. Reeder, and M. Samimy, Control of an axisymmetric jet using vortex generators, Phys. Fluids **6**, 778 (1994).

[5] J. M. Delery, Aspects of vortex breakdown, Prog. Aerosp. Sci. **30**, 1 (1994).

[6] I. M. Kalkhoran, M. K. Smart, and F. Y. Wang, Supersonic vortex breakdown during vortex/cylinder interaction, J. Fluid Mech. **369**, 351 (1998).

[7] T. Hiejima, Criterion for vortex breakdown on shock wave and streamwise vortex interactions, Phys. Rev. E **89**, 053017 (2014).

[8] T. Hiejima, Linear stability analysis on supersonic streamwise vortices, Phys. Fluids **25**, 114103 (2013).

[9] D. Liepmann and M. Gharib, The role of streamwise vorticity in the near-field entrainment of round jets, J. Fluid Mech. **245**, 643 (1992).
[10] I. A. Waitz, Y. J. Qiu, T. A. Manning, A. K. S. Fung, J. K. Elliot, J. M. Kerwin, J. K. Krasnodebski, M. N. O'Sullivan, D. E. Tew, E. M. Greitzer, F. E. Marble, C. S. Tan, and T. G. Tillman, Enhanced mixing with streamwise vorticity, Prog. Aerosp. Sci. **33**, 323 (1997).
[11] T. Sunami, M. Wendt, and M. Nishioka, in *Proceedings of the 34th AIAA/ASME/SAE/ASEE Joint Propulsion Conference and Exhibit* (AIAA, Reston, VA, 1998).
[12] M. Nishioka, S. Sakaue, K. Komada, H. Sakoshi, and I. Furukawa, in *IUTAM Symposium on Elementary Vortices and Coherent Structures: Significance in Turbulence Dynamics*, edited by S. Kida, Fluid Mechanics and its Applications Vol. 79 (Springer Netherlands, Berlin, 2006), pp. 249–258.
[13] L. Maddalena, F. Vergine, and M. Crisnti, Vortex dynamics studies in supersonic flow: Merging of co-rotating streamwise vortices, Phys. Fluids **26**, 046101 (2014).
[14] B. Rust, P. Gerlinger, and M. Aigner, in *Proceedings of the 46th AIAA/ASME/SAE/ASEE Joint Propulsion Conference and Exhibit* (AIAA, Reston, VA, 2010).
[15] T. Sunami, A. Murakami, K. Kudo, M. Kodera, and M. Nishioka, Mixing and combustion control strategies for efficient scramjet operation in wide range of flight Mach number, in *Proceedings of AIAA/AAAF 11th International Space Planes and Hypersonic Systems and Technologies Conference* (AIAA, Reston, VA, 2002).
[16] C. Fureby, K. Nordin-Bates, K. Petterson, A. Bresson, and V. Sabelnikov, A computational study of supersonic combustion in strut injector and hypermixer flow fields, Proc. Combust. Instit. **35**, 2127 (2015).
[17] T. Hiejima, Effects of streamwise vortex breakdown on supersonic combustion, Phys. Rev. E **93**, 043115 (2016).
[18] M. Kodera, T. Sunami, and F. Scheel, Numerical study on the supersonic mixing enhancement using streamwise vortices, in *Proceedings of AIAA/AAAF 11th International Space Planes and Hypersonic Systems and Technologies Conference* (AIAA, Reston, VA, 2002).
[19] A. H. Shapiro, *The Dynamics and Thermodynamics of Compressible Fluid Flow* (Ronald, New York, 1953), Vol. II.
[20] S. Chakravarthy and S. Osher, A new class of high accuracy TVD schemes for hyperbolic conservation laws, in *Proceedings of 23rd Aerospace Sciences Meeting* (AIAA, Reston, VA, 1985).
[21] D. P. Rizzetta, Numerical simulation of vortex-induced oblique shock-wave distortion, AIAA J. **35**, 209 (1997).
[22] J. Délery and J.-P. Dussauge, Some physical aspects of shock wave/boundary layer interactions, Shock Waves **19**, 453 (2009).
[23] J. Jeong and F. Hussain, On the identification of a vortex, J. Fluid Mech. **285**, 69 (1995).
[24] T. Hiejima, Stability of compressible streamwise vortices, Phys. Fluids **27**, 074107 (2015).
[25] H. Schlichting and K. Gersten, *Boundary-Layer Theory*, 8th ed. (Springer, Berlin, 2000).
[26] G. L. Korolev, J. S. B. Gajjar, and A. I. Ruban, Once again on the supersonic flow separation near a corner, J. Fluid Mech. **463**, 173 (2002).
[27] B. Di Pierro and M. Abid, Energy spectra in a helical vortex breakdown, Phys. Fluids **23**, 025104 (2011).
[28] P. E. Dimotakis, The mixing transition in turbulent flows, J. Fluid Mech. **409**, 69 (2000).
[29] F. Holzäpfel, T. Hofbauer, D. Darracq, H. Moet, F. Garnier, and C. F. Gago, Analysis of wake vortex decay mechanisms in the atmosphere, Aerosp. Sci. Technol. **7**, 263 (2003).
[30] H. Moet, F. Laporte, G. Chevalier, and T. Poinsot, Wave propagation in vortices and vortex bursting, Phys. Fluids **17**, 054109 (2005).
[31] H. W. Riepmann and A. Roshko, *Elements of Gasdynamics* (Wiley, New York, 1957), Vol. II.
[32] I. Delbende and M. Rossi, Nonlinear evolution of a swirling jet instability, Phys. Fluids **17**, 044103 (2005).
[33] P. Orlandi and G. F. Carnevale, Evolution of isolated vortices in a rotating fluid of finite depth, J. Fluid Mech. **381**, 239 (2014).
[34] T. Hiejima, Spatial evolution of supersonic streamwise vortices, Phys. Fluids **26**, 074102 (2014).
[35] T. Hiejima, Instability of isolated hollow vortices with zero circulation, Phys. Fluids **28**, 044104 (2016).